INDUCED CHARGE COMPUTATION METHOD

Application in Monte Carlo simulations of inhomogeneous dielectric systems

D. Boda [1], D. Gillespie[2], B. Eisenberg[2], W. Nonner[3], D. Henderson[4]

[1] *Department of Physical Chemistry,*
University of Veszprém,
H–8201 Veszprém, P.O. Box 158, Hungary

[2] *Department of Molecular Biophysics and Physiology,*
Rush University Medical Center,
Chicago, Illinois 60612, USA

[3] *Department of Physiology and Biophysics,*
University of Miami School of Medicine,
Miami, Florida 33101, USA

[4] *Department of Chemistry and Biochemistry,*
Brigham Young University,
Provo, Utah 84602, USA

Abstract   In a recent publication we have introduced the induced charge computation (ICC) method for the calculation of polarization charges induced on dielectric boundaries. It is based on the minimization of an appropriate functional. The resulting solution produces an integral equation that is transformed into a linear matrix equation after discretization. In this work, we discuss the effect of careful calculation of the matrix element and the potential by treating the polarization charges as constant surface charges over the various surface elements. The correct calculation of these quantities is especially important for curved surfaces where mutual polarization of neighboring surface elements is considerable. We report results for more complex geometries including dielectric spheres and an ion channel geometry with a surface of revolution.

Keywords: Dielectric boundaries, Monte Carlo simulation, polarization charge

1.   Introduction

Understanding the behavior of physical systems containing many degrees of freedom requires considerable computational time unless we treat a certain portion of the degrees of freedom as continuous response functions. These

response functions vary widely depending on the interactions they are intended to replace (electrostatic, dispersion, repulsion) and on the nonlocal nature of the medium (uniform homogeneous, inhomogeneous, anisotropic response functions). Because electrostatic interactions play a basic role in many fields such as molecular biology, quantum chemistry, electrochemistry, chemical engineering, and colloid chemistry (without any claim of this being a complete list), one of the most important response functions is the dielectric response of fast atomic and molecular motions. This procedure uses constitutive relations and macroscopic conservation laws and reduces to solving the Poisson's equation for source charges (which are the degrees of freedom treated explicitly) in an inhomogeneous dielectric medium characterized by a space dependent dielectric coefficient, $\varepsilon(\mathbf{r})$.

One field where such a procedure is commonly used is the study of solvation of molecules. The solute (which can be treated quantum mechanically) is hosted in a cavity built in a dielectric continuum representing the solvent. This approach is called the polarizable continuum model (PCM) [1–3] which is studied by the apparent surface charge (ASC) method. This approach determines the surface charge induced on the surface of the cavity so that the appropriate boundary conditions are fulfilled at the boundaries. Using Green's functions, the problem can be written in the integral equation formalism (IEF) [4–6], whose numerical solution results in a linear matrix equation. This matrix equation was first developed by Hoshi et al. [7] and named the boundary element method (BEM). Later Cammi and Tomasi [8, 9] adopted the method of Hoshi et al. and the group of Tomasi have developed several numerical procedures for the fast solution of the matrix equation using various iterative methods [10]. The PCM has been extended to cases where the molecule is hosted in anisotropic solvents, ionic solutions, at liquid interfaces and metals [11]. There are a large number of studies using various BEM procedures including those implementing a linear interpolation across each boundary element to improve accuracy [12–18].

Another field where dielectric continuum models are extensively used is the statistical mechanical study of many particle systems. In the past decades, computer simulations have become the most popular statistical mechanical tool. With the increasing power of computers, simulation of full atomistic models became possible. However, creating models of full atomic detail is still problematic from many reasons: (1) computer resources are still unsatisfactory to obtain simulation results for macroscopic quantities that can be related to experiments; (2) unknown microscopic structures; (3) uncertainties in developing intermolecular potentials (many-body correlations, quantum-corrections, potential parameter estimations). Therefore, creating continuum models, which process is sometimes called "coarse graining" in this field, is still necessary.

The most obvious example is the so called restricted primitive model (RPM) of electrolytes where the ions are represented as charges hard spheres, while the solvent is modelled as a dielectric continuum. Examples for inhomogeneous systems include electrochemical interfaces [19], semiconductor junctions [20], and cell membranes [21, 22].

A biologically crucial field where dielectric continuum models have a basic importance is ion channels embedded in the cell membrane. Several works have been published that use various methods to solve Poisson's equation for channel-like geometries. These include interpolation methods using lookup tables to store discretized Green's functions [23–27], BEM procedures [28–30], generalized multipolar basis-set expansion of the Green's function [31], and analytical solutions [30, 32–34]. The statistical mechanical methods also have a wide variety including the Poisson-Nernst-Planck (PNP) equation [32, 35, 36], Brownian dynamics (BD) simulations [23, 25, 26, 29, 31, 35, 36], the mean spherical approximation (MSA) for homogeneous fluids [37, 38], and Monte Carlo (MC) simulations [34, 39–42]. Special attention must be paid to the MC simulation works of Green and Lu [44–46] who developed a method to calculate dielectric boundary forces that practically equivalent to the BEM resulting in a matrix equation that corresponds to that developed by Hoshi et al. [7].

Ion channel studies motivated Allen et al. [47] who have developed an elegant variational formalism to compute polarization charges induced on dielectric interfaces. They solved the variational problem with a steepest descent method and applied their formulation in molecular dynamics (MD) simulations of water permeation through nanopores in a polarizable membrane [48–50]. Note that the functional chosen by Allen et al. [47] is not the only formalism that can be used. Polarization free energy functionals [51–53] are more appropriate for dynamical problems, such as macromolecule conformational changes and solvation [54–57].

In our two previous papers [58, 59] the induced charge computation (ICC) method for the calculation of polarization charges in an inhomogeneous dielectric system has been introduced. The method is based on the variational formulation of Allen et al. [47]. We have developed a different solution [58] for the minimization of their functional. The discretization of the resulting integral equation leads to a matrix equation that can be readily applied in a computer simulation. Further simplification of the method for the special cases where the source charges are point charges and the dielectric interfaces are sharp boundaries leads to the matrix equation of Hoshi et al. [7] and Green and Lu [44]. We have implemented the method and proved its usefulness in MC simulations of hard sphere ions in simple inhomogeneous dielectric geometries, where the dielectric boundaries are planar [58]. We have presented results for a system for which an analytic solution is available (one flat sharp

boundary), and we have shown that our ICC method provides results in excellent agreement with the simulations using the exact solution (on the basis of electrostatic image charges). Furthermore, we have reported results for the more general case of two parallel flat sharp boundaries (slab geometry) where the matrix is not diagonal.

The generalization of ICC method allows to impose arbitrary boundary conditions on various boundaries in the system [59]. Furthermore, a numerical approach to calculate the surface integrals appearing in the matrix elements has also been introduced [59]. The correct calculation of these integrals is especially important in the case of curved surfaces; therefore, it is sometimes called "curvature correction". In this work, we present the method of [58] supplemented by the "curvature corrections" introduced in [59] and we report results for more complex geometries than those considered in [58]. We show that "curvature corrections" are important not only for curved surfaces but also for the slab geometry if the slab is thin. We study the potential of a charge in a dielectric sphere and show results for the effective interaction between two charged dielectric spheres. We also show some preliminary results for a calcium channel that have a rotational geometry.

2.   Method

2.1   *Variational formulation*

Let us consider a discrete or continuous charge distribution $\rho(\mathbf{r})$ confined to a domain $\mathcal{D}$ of volume V with a boundary $\mathcal{S}$. For the geometries considered in this work, the potential can be chosen to be vanishingly small on $\mathcal{S}$. This makes the elimination of some surface terms possible. This does not mean that we impose zero potential on the boundary of the system. Instead, we use infinite systems (simply assuming that the system is infinite, or, in the case of simulation, applying periodic boundary condition), or, in the case of a finite simulation cell, we assume that the cell is large enough that the potential is small on the boundary in average. Nevertheless, the method has been generalized by Nonner and Gillespie [59] that makes it possible to directly impose arbitrary boundary conditions on the boundaries of the system. This generalization is not considered in this paper.

In the case of an inhomogeneous dielectric, we separate the total charge distribution into two parts. We treat only a fraction of the charges explicitly, this part of the charge density is called source (or external, or free) charge distribution, and it is denoted by $\rho(\mathbf{r})$. The rest of the degrees of freedom, corresponding usually to fast atomic and molecular motions, is replaced by their dielectric response using a constitutive relation. In the presence of an external electric field the dielectric matter containing the charges other than the source charges is polarized. If the dielectric response is linear, the polarization

$\mathbf{P}(\mathbf{r})$ produced by an electric field $\mathbf{E}(\mathbf{r})$ can be given as,

$$\mathbf{P}(\mathbf{r}) = \varepsilon_0 \chi(\mathbf{r})\mathbf{E}(\mathbf{r}) = -\varepsilon_0 \chi(\mathbf{r})\nabla\psi(\mathbf{r}) \,, \tag{1}$$

where $\chi(\mathbf{r})$ is the dielectric susceptibility. The dielectric susceptibility is space-dependent that characterizes an inhomogeneous dielectric in the domain $\mathcal{D}$. This corresponds to a local relative permittivity $\varepsilon(\mathbf{r}) = 1 + \chi(\mathbf{r})$. In general, this is a tensor, but in this work we restrict ourselves to a scalar relative permittivity ($\mathbf{P}$ and $\mathbf{E}$ have the same directions). For the case of a bulk system, this quantity is called dielectric constant; in this work we use the term dielectric coefficient to emphasize that it is not constant in space. The polarization charge density induced by the source charge distribution is associated with the potential through,

$$\rho_{\text{pol}}(\mathbf{r}) = -\nabla \cdot \mathbf{P}(\mathbf{r}) = \varepsilon_0 \nabla \cdot [\chi(\mathbf{r})\nabla\psi(\mathbf{r})] \,. \tag{2}$$

Introducing the normalized versions of the source and the polarization charge densities,

$$g(\mathbf{r}) = \frac{\rho(\mathbf{r})}{\varepsilon_0} \,, \tag{3}$$

and

$$h(\mathbf{r}) = \frac{\rho_{\text{pol}}(\mathbf{r})}{\varepsilon_0} \,, \tag{4}$$

Poisson's equation can be given as,

$$\nabla^2 \psi(\mathbf{r}) = -\left[g(\mathbf{r}) + h(\mathbf{r})\right] \,, \tag{5}$$

and the corresponding functional [47] is,

$$I\left[\psi\right] = \frac{1}{2}\int_{\mathcal{D}} \nabla\psi \cdot \nabla\psi \mathrm{d}\mathbf{r} - \int_{\mathcal{D}} \psi \left[g + \frac{1}{2}\nabla \cdot (\chi\nabla\psi)\right] \mathrm{d}\mathbf{r} \,. \tag{6}$$

In order to express $I[\psi]$ as a functional of the polarization charge density, the potential is also split into the "external" and the "induced" parts which are expressed in terms of $g(\mathbf{r})$ and $h(\mathbf{r})$ with the help of the Green's function as,

$$\begin{aligned}\psi(\mathbf{r}) &= \psi_{\text{e}}(\mathbf{r}) + \psi_{\text{i}}(\mathbf{r}) = \\ &= \int_{\mathcal{D}} G(\mathbf{r} - \mathbf{r}')g(\mathbf{r}')\mathrm{d}\mathbf{r}' + \int_{\mathcal{D}} G(\mathbf{r} - \mathbf{r}')h(\mathbf{r}')\mathrm{d}\mathbf{r}',\end{aligned} \tag{7}$$

where the Green's function satisfies,

$$\nabla^2 G(\mathbf{r} - \mathbf{r}') = -\delta(\mathbf{r} - \mathbf{r}') \,, \tag{8}$$

with $\delta(\mathbf{r} - \mathbf{r}')$ being the Dirac delta function. Substituting Eq. (7) into Eq. (6), the functional can be given as a function of $g(\mathbf{r})$, $h(\mathbf{r})$, and $\psi_{\mathrm{e}}(\mathbf{r})$, e. g. $I = I[g, h, \psi_{\mathrm{e}}]$. The task is to determine the polarization charge density $h(\mathbf{r})$ for a given external charge density $g(\mathbf{r})$ that satisfies Eq. (5), or, equivalently, minimizes $I[g, h, \psi_{\mathrm{e}}]$. Determining $h(\mathbf{r})$ for a fixed $g(\mathbf{r})$ is equivalent to minimizing the h-dependent part of the functional $I[g, h, \psi_{\mathrm{e}}]$, which is denoted by $I_2[h]$. Allen et al. [47] showed that the extremum condition,

$$\frac{\delta I_2[h]}{\delta h(\mathbf{r})} = 0\,, \tag{9}$$

leads back to the constitutive relation in Eq. (1), that the extremum is a minimum, and that the value of $I[h]$ at the minimum reduces to minus the electrostatic energy. Allen *et al.* [47] solved the variational problem (after discretization) with a steepest descent method. In our previous work [58], we have proposed a different route that results in the integral equation,

$$h(\mathbf{r})\varepsilon(\mathbf{r}) - \int_{\mathcal{D}} h(\mathbf{r}')\nabla_{\mathbf{r}}\varepsilon(\mathbf{r}) \cdot \nabla_{\mathbf{r}}G(\mathbf{r} - \mathbf{r}')\mathrm{d}\mathbf{r}' =$$
$$= \nabla_{\mathbf{r}}\varepsilon(\mathbf{r}) \cdot \nabla_{\mathbf{r}}\psi_{\mathrm{e}}(\mathbf{r}) - [\varepsilon(\mathbf{r}) - 1]\, g(\mathbf{r})\,. \tag{10}$$

Discretizing the central equation (Eq. (10)) of the ICC method leads to a matrix equation. In this work, we focus on the case of sharp dielectric boundaries, therefore, we will show the details of discretization for that case. To our knowledge, this equation for the general case $\varepsilon(\mathbf{r})$ has not been derived previously. Recently, Frediani et al. [11] has reported an integral equation for the case of a molecule solvated at a diffuse interface between two fluid phases (liquid/liquid or liquid/vapor). Their interface is described by a dielectric profile $\varepsilon(z)$ that is a continuous function of the z coordinate, while the charge distribution of the molecule is placed in a cavity formed in the diffuse interface. An integral equation has been developed by Frediani et al. by finding the appropriate Green's function through certain integral operators. The resulting equation is similar to Eq. (10), but is less general.

2.2   *Discrete, point source charges*

When the source charges are point charges in discrete locations, the source charge density is given by

$$g(\mathbf{r}) = \frac{e}{\varepsilon_0} \sum_k z_k \delta(\mathbf{r} - \mathbf{r}_k), \tag{11}$$

where source charge k with valence z_k is located at $\mathbf{r}_k$ and e is the elementary charge. Because these charges have no surface area, the induced charge

around each point charge k is localized at its position $\mathbf{r}_k$. Assuming that the dielectric is locally uniform around the source charge $z_k e$ with dielectric coefficient $\varepsilon(\mathbf{r}_k)$, the magnitude of the induced charge is $-z_k e[\varepsilon(\mathbf{r}_k) - 1]/\varepsilon(\mathbf{r}_k)$ [60]. Therefore, the contribution to h from the induced charges around the source charges is,

$$h'(\mathbf{r}) = -\frac{e}{\varepsilon_0} \sum_k z_k \, \frac{\varepsilon(\mathbf{r}_k) - 1}{\varepsilon(\mathbf{r}_k)} \, \delta(\mathbf{r} - \mathbf{r}_k) \,. \tag{12}$$

Let us consider the source point charges $g(\mathbf{r})$ and the induced charges $h'(\mathbf{r})$ localized on them together; and let us denote the sum of these two terms by $g(\mathbf{r})$ hereafter. In other words, we move $h'(\mathbf{r})$ from the group of induced charges to the group of source charges. Accordingly, the electric potential raised by $h'(\mathbf{r})$ also contributes to the potential of the source point charges; the sum of the two potentials is denoted by ψ_e henceforth. It can be shown that for the resulting potential,

$$\nabla^2 \psi_e(\mathbf{r}) = -\big[g(\mathbf{r}) + h'(\mathbf{r})\big] = -\frac{e}{\varepsilon_0} \sum_k \frac{z_k}{\varepsilon(\mathbf{r}_k)} \, \delta(\mathbf{r} - \mathbf{r}_k) \,, \tag{13}$$

applies from which this potential is expressed as,

$$\psi_e(\mathbf{r}) = \frac{e}{4\pi\varepsilon_0} \sum_k \frac{z_k}{\varepsilon(\mathbf{r}_k)|\mathbf{r} - \mathbf{r}_k|} \,. \tag{14}$$

The dielectric coefficient $\varepsilon(\mathbf{r}_k)$ at the place of charge k appears in the denominator. This corresponds to a dielectric screening that is conventionally used in various descriptions of electrolytes where the solvent is interpreted as a dielectric continuum background (for instance, in the Debye-Hückel theory, in the Gouy-Chapman theory, or in the RPM of electrolyte solutions).

Substituting the redefined $g(\mathbf{r})$ and $\psi_e(\mathbf{r})$ into Eq. (10), we obtain,

$$h(\mathbf{r})\varepsilon(\mathbf{r}) - \int_{\mathcal{D}} h(\mathbf{r}')\nabla_{\mathbf{r}}\varepsilon(\mathbf{r}) \cdot \nabla_{\mathbf{r}} G(\mathbf{r} - \mathbf{r}')d\mathbf{r}' = \nabla_{\mathbf{r}}\varepsilon(\mathbf{r}) \cdot \nabla_{\mathbf{r}}\psi_e(\mathbf{r}), \tag{15}$$

where $h(\mathbf{r})$ refers solely to the induced charges other than $h'(\mathbf{r})$.

It is important to note that if the source charge were an ion represented, for example, as a point charge at the center of a hard dielectric sphere (with a dielectric coefficient different from that of the surrounding medium), then the induced charge on the ion surface must also be determined (as in the case of ASC methods); this would be another contribution to $h(\mathbf{r})$ on the LHS of Eq. (10). Since in a computer simulation the source charges are moving compared to the dielectric surfaces, the geometry of the dielectric pattern would constantly change, which, in turn, would make the computation time consuming. There-

fore, in the simulations, we assume that the interior of the ion has the same dielectric coefficient as the surrounding medium. For the same reason, we assume that the ions move in regions of constant dielectric coefficient, namely, they do not overlap with dielectric boundaries and they are not displaced from one dielectric domain to another. In this work, we will show results for the cases where the interior of an ion has different dielectric coefficient than that of the surrounding medium.

2.3   *Sharp dielectric boundaries*

In the special case of sharp dielectric boundaries the dielectrics is separated into domains of uniform dielectric coefficients. The dielectric coefficient jumps from one value to another along a boundary. Let us denote the surface of the dielectric boundaries by $\mathcal{B}$. Then the induced charge is a surface charge on the dielectric interfaces (if the induced charges around the source charges are not considered), and the volume integral in Eq. (15) becomes a surface integral over the surface $\mathcal{B}$,

$$h(\mathbf{s})\varepsilon(\mathbf{s}) - \Delta\varepsilon(\mathbf{s})\int_{\mathcal{B}} h(\mathbf{s}')\nabla_{\mathbf{s}}G(\mathbf{s}-\mathbf{s}')\cdot\mathbf{n}(\mathbf{s})\mathrm{d}\mathbf{s}' = \Delta\varepsilon(\mathbf{s})\nabla\psi_{\mathrm{e}}(\mathbf{s})\cdot\mathbf{n}(\mathbf{s})\,, \quad (16)$$

where the dielectric coefficient $\varepsilon(\mathbf{s})$ on the boundary is defined to be the arithmetic mean of the two dielectric coefficients on each side of the boundary. Furthermore, the dielectric jump $\Delta\varepsilon(\mathbf{s})$ is the difference of the two dielectric coefficients on each side of the boundary in the direction of the local unit normal of the surface $\mathbf{n}(\mathbf{s})$.

To solve Eq. (16) numerically, the surface $\mathcal{B}$ must be discretized; specifically, each discrete surface element $\mathcal{B}_{\alpha}$ of $\mathcal{B}$ is characterized by its center-of-mass $\mathbf{s}_{\alpha}$, area a_{α}, unit normal $\mathbf{n}_{\alpha} = \mathbf{n}(\mathbf{s}_{\alpha})$, value of the mean dielectric coefficient $\varepsilon_{\alpha} = \varepsilon(\mathbf{s}_{\alpha})$, and value of the dielectric jump $\Delta\varepsilon_{\alpha} = \Delta\varepsilon(\mathbf{s}_{\alpha})$. Due to the assumption of the vanishingly small potential on $\mathcal{S}$, the Green's function simply is,

$$G(\mathbf{s}-\mathbf{s}') = \frac{1}{4\pi|\mathbf{s}-\mathbf{s}'|}. \quad (17)$$

Also, since the density of the discrete point charges is given, the resulting potential ψ_{e} is known from Eq. (14). Of course, $\nabla_{\mathbf{s}}G(\mathbf{s}-\mathbf{s}')$ and $\nabla\psi_{\mathrm{e}}(\mathbf{s})$ are also known. The otherwise continuous surface charge density $h(\mathbf{s})$ is then discretized into certain constant values $h_{\alpha} = h(\mathbf{s}_{\alpha})$ taken on the surface element $\mathcal{B}_{\alpha}$.

Eq. (16) is valid for any vector $\mathbf{s}$. If we rewrite the equation for the discrete values of the centers of the surface elements $\mathbf{s}_{\alpha}$, the surface integral in Eq. (16) becomes a sum of surface integrals over the surface elements $\mathcal{B}_{\beta}$. Using the

assumption that h_β is constant over $\mathcal{B}_\beta$, we obtain for a given α that,

$$\sum_\beta h_\beta \left[\varepsilon_\beta \delta_{\alpha\beta} - \Delta\varepsilon_\alpha \int_{\mathcal{B}_\beta} \nabla_{\mathbf{s}_\alpha} G(\mathbf{s}_\alpha - \mathbf{s}_\beta) \cdot \mathbf{n}_\alpha \mathrm{d}\mathbf{s}_\beta \right] =$$
$$= \Delta\varepsilon_\alpha \nabla\psi_\mathrm{e}(\mathbf{s}_\alpha) \cdot \mathbf{n}_\alpha, \quad (18)$$

where $\delta_{\alpha\beta}$ is the Kronecker δ. This can be rewritten in a matrix form as,

$$A\mathbf{h} = \mathbf{c}, \quad (19)$$

where each element of the matrix A is given by the expression in square brackets,

$$A_{\alpha\beta} = \varepsilon_\beta \delta_{\alpha\beta} - \Delta\varepsilon_\alpha I_{\alpha\beta}, \quad (20)$$

where $I_{\alpha\beta}$ denotes the integral in Eq. (18). Each element of the column vector $\mathbf{h}$ is given by h_β and each element of the column vector $\mathbf{c}$ is given by the right hand side of Eq. (18),

$$c_\alpha = \Delta\varepsilon_\alpha \nabla\psi_\mathrm{e}(\mathbf{s}_\alpha) \cdot \mathbf{n}_\alpha. \quad (21)$$

For the calculation of the integral $I_{\alpha\beta}$, there are two levels of approximation to interpret the charge on a surface element. The first route is to consider the surface charge as a point charge of magnitude $h_\beta a_\beta$ localized at $\mathbf{s}_\beta$. We call this approach the *point charge* (PC) approximation. In this case the integral reduces to an interaction term between point charges,

$$I_{\alpha\beta} = \nabla_{\mathbf{s}_\alpha} G(\mathbf{s}_\alpha - \mathbf{s}_\beta) \cdot \mathbf{n}_\alpha a_\beta \quad (22)$$

for $\beta \neq \alpha$ and 0 otherwise (an induced point charge does not polarize itself). This approach was used in our previous work [58], where we tested the method on planar dielectric interfaces.

On the higher level of approximation, the induced charge on the βth surface element is considered as a surface charge with the constant value h_β. This approach, which we call the *surface charge* (SC) approximation, was introduced in [59]. The main difference is geometrical: the values of the integrals in Eq. (18) do not depend on charges, they depend only on the geometry of the dielectric boundary surfaces and the way they are discretized. The integral represents the polarization of the induced charges on the surface element $\mathcal{B}_\beta$ by the induced charge at $\mathbf{s}_\alpha$. Practically, this approach means that we have to evaluate the surface integrals $I_{\alpha\beta}$. This is a numerical problem; a procedure to solve it was proposed in [59]. We parametrize the two-dimensional surface $\mathcal{B}_\beta$ by two variables u and v. There is a transformation that converts u and v into Cartesian coordinates: $x = X(u,v)$, $y = Y(u,v)$, and $z = Z(u,v)$.

Therefore, both $G(\mathbf{s}_\alpha - \mathbf{s}_\beta)$ and $\mathbf{n}(\mathbf{s}_\alpha)$ can be expressed in terms of the new parameters: $G(u_\alpha, v_\alpha, u_\beta, v_\beta)$ and $\mathbf{n}(u_\alpha, v_\alpha)$. Let us discretize the βth surface element into subelements by evenly dividing the variables u_β and v_β into subintervals of widths Δu_β and Δv_β. Then, the integral can be calculated as,

$$I_{\alpha\beta} = \sum_k \sum_l \nabla_\alpha G(u_\alpha, v_\alpha, u_{\beta,k}, v_{\beta,l}) \cdot \mathbf{n}(u_\alpha, v_\alpha) \; a(u_{\beta,k}, v_{\beta,l}) \, \Delta u_\beta \, \Delta v_\beta \,,$$

(23)

where $a(u_{\beta,k}, v_{\beta,l})$ denotes the area element and $(u_{\beta,k}, v_{\beta,l})$ gives the center of the k, lth subelement of the βth surface element. Also, care must be taken to ensure that $u_\alpha \neq u_{\beta,k}$ and $v_\alpha \neq v_{\beta,l}$.

It has been realized before that the convergence of the results with increasing the resolution of the grid is poor using the PC approximation. A curvature correction was used by many workers [1, 3, 7, 23, 24], where an empirical parameter was built into the diagonal elements of the matrix (for reviews, see [18, 61]). Instead of this uncertain parameter, it is more appropriate to evaluate the integrals numerically. In our SC approximation, the integrals are computed by assuming that the surface charge is constant within a surface element. A higher level approximation was used in several works [12–18] where the surface charge within a surface element is interpolated from the surface charges in the neighboring tiles. Recently, Chen and Chipman [18] have proposed a linear interpolation method using a triangulation of the surface. The sample points ($\mathbf{s}_\alpha$) are the corners of the triangles, and the integrals over the triangles are evaluated by interpolating the surface charge inside a triangle from those at the three corners. The development of a similar interpolation method for our parametrization procedure using the u, v parameters is under way.

The evaluation of the integrals in the SC approximation is quite time consuming. Nevertheless, the speed of filling and inverting the matrix is not an issue in computer simulations if the geometry of the dielectric boundaries does not change during the simulation. Thus, the inverse of A (or any factorization of A) need only be computed *once* for a given geometry and dielectric profile. The calculation of $I_{\alpha\beta}$ by subdiscretizing the surface elements does not increase the *size* of the matrix, it only influences the *fill time* of the matrix, which is also performed once at the beginning of a simulation.

Note that two points situated on a planar surface do not polarize each other. Therefore, it is expected that for planar interfaces the method of the calculation of the integral $I_{\alpha\beta}$ has smaller effect on the accuracy of the method. Indeed, in our previous work [58], we have obtained satisfactory results for one planar and two parallel planar interfaces using the PC approximation. In the case of curved surfaces, the accurate calculation of $I_{\alpha\beta}$ is very important as we will show for spherical and cylindrical geometries in the Results section.

2.4   *Calculation of the energy*

In an MC simulation the essential quantity is the change in the energy of the system in an MC step. The MC step is normally a stochastic particle displacement, chosen from a uniform distribution, but biased moves are also possible [62–65]. Some details of our MC simulations will be given in the Results section, here we give the procedure with which the electrostatic energy is calculated in the framework the ICC method. We assume that the source charges are point charges and that the dielectric boundaries are sharp as described in the preceding two subsections.

The electrostatic energy can be split into two parts. The source charge – source charge interaction energy is,

$$W_{\mathrm{e}} = \frac{1}{2} \sum_j e z_j \psi_{\mathrm{e}}(\mathbf{r}_j) \,, \tag{24}$$

where the electrostatic potential of the source point charges is given by Eq. (14). The source charge – induced charge interaction is given by,

$$W_{\mathrm{i}} = \frac{e}{8\pi} \sum_j z_j \int_{\mathcal{B}} \frac{h(\mathbf{s})}{|\mathbf{s} - \mathbf{r}_j|} \mathrm{d}\mathbf{s} \,. \tag{25}$$

After discretization, as in the case of filling the matrix, we have two choices in the calculation of the above integral. In the PC approximation the integral becomes a sum of point charge – point charge interactions,

$$W_{\mathrm{i}} = \frac{e}{8\pi} \sum_j z_j \sum_\beta \frac{h_\beta a_\beta}{|\mathbf{s}_\beta - \mathbf{r}_j|} \,. \tag{26}$$

In the above equations, the indices j and β range over the source point charges and the surface elements, respectively. In the SC approximation the integral expresses a point charge – surface charge interaction,

$$W_{\mathrm{i}} = \frac{e}{8\pi} \sum_j z_j \sum_\beta h_\beta \int_{\mathcal{B}_\beta} \frac{\mathrm{d}\mathbf{s}}{|\mathbf{s} - \mathbf{r}_j|} \,. \tag{27}$$

The integral in Eq. (27) is a geometrical term similarly to $I_{\alpha\beta}$ in Eq. (18) and it can be calculated similarly by the parametrization procedure outlined in the previous subsection. The problem with the SC route is that the integral has to be recalculated for the jth ion every time when it is displaced in the MC step. This would slow the simulations down considerably. Fortunately, as we will see from the results shown in the next section, this integral is important only if the charge is very close to the dielectric boundary. Since we simulate

ions with a finite diameter and the ion centers (where the source charges are located) cannot approach the surface closer than the half of the ionic diameter, this problem does not arise in our simulations.

In a usual MC simulation we use single particle movements, namely, only one particle is displaced in an MC step. This fact and the linearity of the matrix equation $A\mathbf{h} = \mathbf{c}$ make it possible to decrease the computation time of the energy change ΔW. This is because the distances between particles that are not moved do not change in the MC step and the distances between these particles and the surface elements are also unchanged. Storing the intermolecular distances in an array, the computational burden can be decreased by saving time consuming square roots. The details can be found in [58].

It is important to note that in our simulations we assume that the ions do not cross the dielectric boundaries. If an ion were to cross a dielectric boundary in the MC step, the energy of interaction of the ion with the two different dielectrics (that corresponds to the solvation energies) must be included. Calculating such energies is difficult. Instead, empirical parameters describing this energy difference might be included in the calculation as in our previous work [34] where we studied the selectivity of a calcium channel where the dielectric coefficient of the selectivity filter was different from that of the bulk electrolyte. Nevertheless, estimating such empirical parameters is still problematic. Therefore, as a first approximation, we avoid this problem and assume that the dielectric boundaries act as hard walls and the ions cannot leave their host dielectrics.

3.   Results

3.1   *Planar geometry*

In the planar geometry we consider a dielectric slab shown in Fig. 1. Two semi-infinite dielectrics of dielectric coefficients ε_1 and ε_3 are separated by a dielectric slab of thickness D and with a dielectric coefficient ε_2. The boundaries of the slab are flat, sharp, and parallel. This can be regarded as a simple model of a membrane. This case has been studied in our previous paper [58] where MC simulation results have been shown for the distribution of hard sphere ions around a slab. Nevertheless, in our previous work, we did not use the SC approximation. In the following, we will show that it is necessary only if the width of the slab is small compared to the width of the surface elements.

When we solve the problem numerically, the number of surface elements, and consequently, the size of the dielectric boundary surfaces must be finite. This is in accordance with the practice in a simulation, where the simulation cell is also finite. To approximate an infinite system in a simulation, periodic boundary conditions are applied in the x and y directions. The closest image convention is used not only for the ionic distances but any distances between
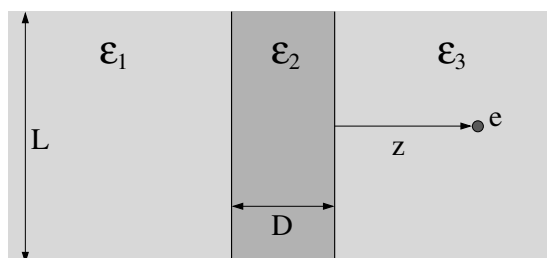
Figure 1.   The slab geometry.

two physical points in the simulation cell including points on the boundary surfaces ($\mathbf{s}_\beta$). Here we show results only for one source point charge. Nevertheless, to remain in connection with simulations, we use two square walls of dimensions $L \times L$, although using circular walls with the charge above the center is also possible. According to periodic boundary conditions, the grids on the surface of the two walls are constructed by evenly dividing them into square elements of width Δx (with $L/\Delta x$ being an integer). This means that the surface elements are parametrized by the x and y variables ($u = x$ and $v = y$). The value of Δx, namely the fineness of the grid, is a crucial point of the calculation (it was discussed in [58] in detail). Briefly, Δx must be small enough compared to the closest approach of a charge to the surface. Furthermore, the dimensions of the simulation cell have to be large enough, which is a usual criteria in computer simulations.

In this work, we concentrate on the issue of what happens if the width of the slab is small. In this case, the induced charges on the left wall are close to the induced charges on the right wall so the effect of their mutual polarization is large. Consequently, the accurate calculation of the $I_{\alpha\beta}$ integral, which represents this mutual polarization, is important. To investigate this effect, we calculate the polarization energy of a single point charge of magnitude e as a function of the distance of the charge from the slab. The polarization energy is the interaction energy between a charge and the polarization charges induced by this charge; this corresponds to W_i in Eq. (25) with $z_1 = 1$ ($j = 1$ because only one charge is present). This is a dominant term in the energy of a many particle system when an ion is close to the boundary, therefore, it is appropriate to test the accuracy of the method. Its precise value depends on the situation of the charge with respect to the surface element as we discussed in detail [58]. Here we calculate the polarization energy assuming that the charge is above the center of a square which corresponds to position 3 in Fig. 3 of [58]. The slab geometry has the advantage that analytical solutions are available in the
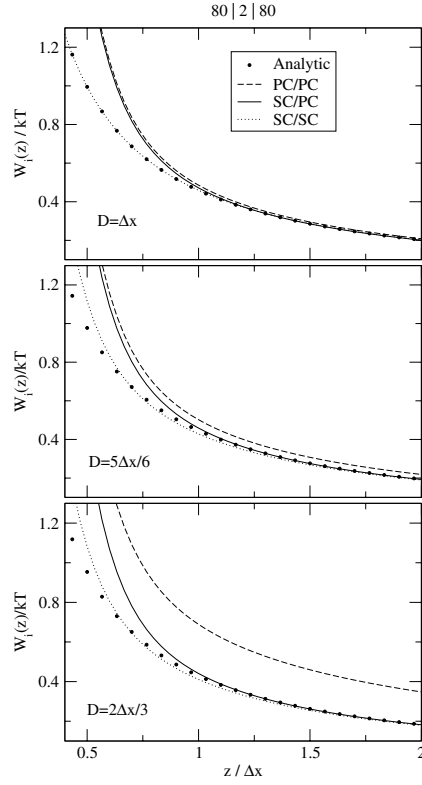
80 | 2 | 80

Figure 2.   The polarization energy W_i of a single charge of magnitude e as a function of the distance of the charge from the slab for different slab widths. The dielectric coefficients of the slab geometry are $\varepsilon_1 = 80; \varepsilon_2 = 2; \varepsilon_3 = 80$. The polarization energy is normalized by kT where $T = 300$ K. The ICC curves as obtained from different approaches (PC/PC, SC/PC, and SC/SC; the explanation of the abbreviations can be found in the main text) are compared to the analytical solution [66].

form of infinite series. Here, we use the formulas given by Allen and Hansen [66].

We consider three possibilities that differ whether we use the PC or the SC approximation in the calculation of $I_{\alpha\beta}$ and/or W_i:

(1) We can use Eq. (22) for the calculation of the matrix element and Eq. (26) for the calculation of W_i, namely, the PC approximation is used in both cases (PC/PC). This approach was used in [58].

(2) Using Eq. (23) for the calculation of the matrix element and Eq. (26) for the calculation of W_i means that the SC approximation is used only to fill the matrix (SC/PC).

(3) If we use Eq. (23) for the calculation of the matrix element and Eq. (27) for the calculation of W_i, the SC approximation is used in both cases (SC/SC). As mentioned before, using Eq. (27) significantly slows the simulation.

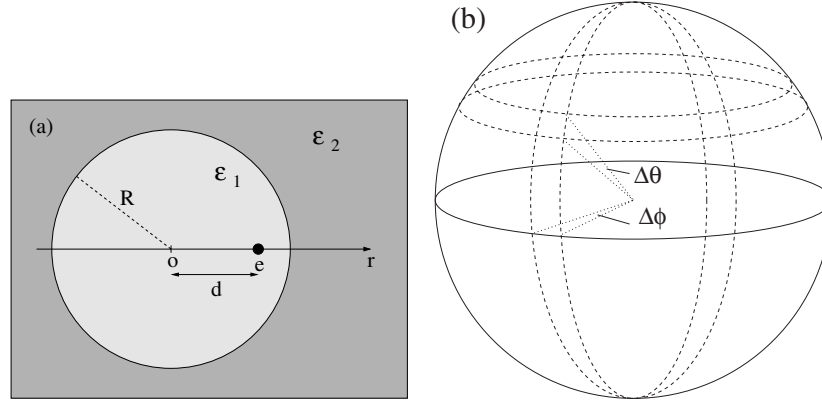These notations will also be used in subsequent subsections.

Figure 3. (a) The geometry of a dielectric sphere of dieletric coefficient ε_1 embedded in a mediun of dielectric coefficient ε_2 with a source point charge within the sphere. (b) The grid on the surface of a sphere is constructed by evenly dividing the spherical coordinates ϕ and θ into subintervals of widths $\Delta\phi$ and $\Delta\theta$.

Figure 2 shows the results for these cases for different values of D. For the width of walls the value $L = 20\Delta x$ is used. The temperature is $T = 300$ K in every calculation in this work. In the PC/PC case (dashed lines) the polarization energy is not reproduced even for large z when the width of the slab is small compared to Δx. In the case of $D = 2\Delta x/3$, the deviation is considerable. Using the SC approximation to fill the matrix (SC/PC), the magnitude of the energy for large z is recovered, but the behavior near the boundary is still bad (solid curves). Using the SC approximation to calculate the energy also (SC/SC), the behavior of the curves becomes much better even for small distances from the boundary. It is worth emphasizing that the SC/SC approach gives good results for $D = \Delta x$, which means that the errors due to different positions of the charge with respect to the grid [58] can be overcome (at least partly) by using the SC approximation to calculate W_i.

3.2 *One dielectric sphere*

A dielectric sphere of dielectric coefficient ε_1 embedded in an infinite dielectric of permittivity ε_2 is an important case from many points of view. The idea of a cavity formed in a dielectric is routinely used in the classical theories of the dielectric constant [67–69]. Such cavities are used in the studies of solvation of molecules in the framework of PCM [1–7] although the shape of the cavities mimic that of the molecule and are usually not spherical. Dielectric spheres are important in models of colloid particles, electrorheological fluids, and macromolecules just to mention a few. Of course, the ICC method is not restricted to a spherical sample, but, for this study, the main advantage of this geometry lies just in its spherical symmetry. This is one of the simplest examples where the dielectric boundary is curved; and an analytic solution is available for this geometry in the form of Legendre polynomials [60]. In the previous subsection, we showed an example where the SC approximation is important while the boundaries are not curved. As mentioned before, using the SC approximation is especially important if we consider curved dielectric boundaries. The dielectric sphere is an excellent example to demonstrate the importance of "curvature corrections".
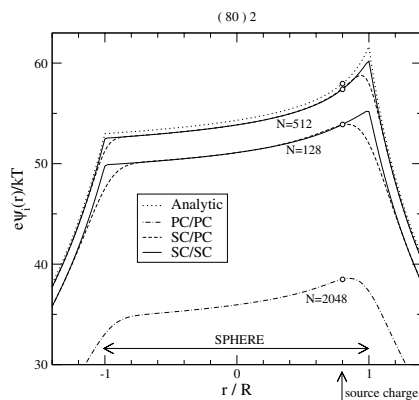

Figure 4. The potential of the induced charges $e\psi_i(r)/kT$ as a function of r along the line crossing the center of the sphere and the source charge. The ICC curves as obtained from different approaches (PC/PC, SC/PC, and SC/SC) are compared to the analytical solution obtained from a series expansion of Legendre polynomials [60].

We will show results for the case where the dielectric coefficient is $\varepsilon_1 = 80$ inside, and $\varepsilon_2 = 2$ outside. For the reverse case, when the sourse charge is in the regime with the higher dielectric coefficient, we would obtain qualitatively similar, quantitatively even better converging results. Because of the

spherical symmetry, the surface of the sphere is parametrized by the spherical coordinates ($u = \theta$ and $v = \phi$). The geometry is shown in Fig. 3a, while the corresponding grid is illustrated in Fig. 3b. A source charge is placed inside the sphere in a distance $d = 0.8R$ from the center of the sphere, where R is the radius of the sphere. Fig. 4 shows the potential produced by the polarization charges induced by the source charge on the surface of the sphere. The dimensionless potential $e\psi_i/kT$ is plotted as a function of r/R, where r is the distance from the center of the sphere along the line through the center and the source charge. The positive direction shows from the center to the source charge. In the case of the PC/PC approach there is a large difference between the analytic and the ICC solutions even for a very large number of surface elements $N = 2048$ (dot-dashed line). If we use the SC approximation to calculate the matrix elements (SC/PC), the agreement with the analytic solution becomes much better, but near the surface of the sphere the ICC curves (dashed lines) fail to reproduce the kinks in the analytic curve (dotted lines). Increasing the number of surface elements (from $N = 128$ to $N = 512$) the ICC curves approach the analytic curve. Using the SC/SC approach, the behavior of the ICC curves becomes satisfactory even in the vicinity of the boundary of the sphere (solid lines).

It is important to determine the centers of the surface elements correctly. If we parametrize the area element α by the variables u and v then the coordinates of the center are calculated as,

$$\overline{u}_\alpha = \frac{\iint_{\mathcal{B}_\alpha} u\, a(u,v)\mathrm{d}u\mathrm{d}v}{\iint_{\mathcal{B}_\alpha} a(u,v)\mathrm{d}u\mathrm{d}v} \, , \tag{28}$$

and similarly for $\overline{v}_\alpha$, where $\overline{\mathbf{s}} = (\overline{u}_\alpha, \overline{v}_\alpha)$ is the center of the tile [59]. The centers of the subelements should be calculated similarly. If we determine the center by simply taking the centers of the Δu_α and Δv_α intervals instead of the above weighted average, we introduce a small error into our calculation. For the example of the one dielectric sphere, the polarization energy ($W_i/kT = e\psi_i(d)/kT$ denoted by open circles in Fig. 4) is 57.4 if we calculate $\overline{\mathbf{s}}$ correctly from Eq. (28) (using 512 tiles), and 57.074 otherwise. The analytical value is 57.9616. Although it is small, this error might be important as in the case of the two spheres in the next subsection.

3.3 *Two dielectric spheres*

As mentioned before, the ions are modelled as point charges embedded in the center of a hard sphere where the sphere has the same dielectric coefficient as the surrounding medium. This approach replaces the polarization charges induced around the source charge from the surface of the sphere to the position of the source charge localized on it. The error made by this assumption was

investigated by Allen and Hansen [70] who used their variational approach to calculate the effective interaction between charges within dielectric cavities. For a few special cases, they have developed solutions for the problems in the form of series expansions without using a grid. The general situation for spherical cavities can be seen in Fig. 5. Two dielectric spheres of radii R_1 and R_2 are immersed in a dielectric of dielectric coefficient ε_3. The dielectric coefficients in the spheres are ε_1 and ε_2. The distance of the centers of the spheres is r. Point charges of magnitudes q_1 and q_2 are placed at the centers of Sphere 1 and 2, respectively.
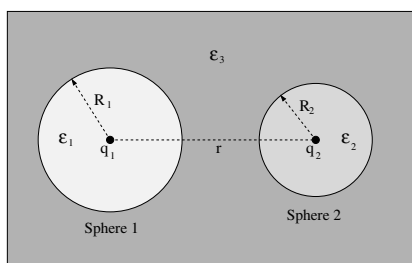

Figure 5.   The geometry for two charges within dielectric spheres.

If the dielectric is homoegeneous ($\varepsilon_1 = \varepsilon_2 = \varepsilon_3$), the interaction potential between the charges is the Coulomb potential divided by ε_3. Introducing the effective dielectric coefficient $\varepsilon_{\text{eff}}(r)$ [70], the interaction potential can be written in the form of the Coulomb potential by

$$V_{\text{int}}(r) = \frac{q_1 q_2}{4\pi\varepsilon_0\, \varepsilon_{\text{eff}}(r)\, r} \tag{29}$$

for the case where dielectric boundaries are present. The interaction potential is defined by the difference,

$$V_{\text{int}}(r) = W(r) - W(\infty), \tag{30}$$

where $W(\infty)$ is the energy of the system when the spheres are infinitely far from each other. This term is the interaction energy between the ions and the polarization charges induced by the charges on their own spheres. This is an "intramolecular" term, while $V_{\text{int}}(r)$ is an "intermolecular" term which goes to zero increasing the distance of the spheres. For the former term an analytical expression exists,

$$W(\infty) = \frac{\varepsilon_1 - \varepsilon_3}{8\pi\varepsilon_0\varepsilon_1\varepsilon_3} \frac{q_1^2}{R_1} + \frac{\varepsilon_2 - \varepsilon_3}{8\pi\varepsilon_0\varepsilon_2\varepsilon_3} \frac{q_2^2}{R_2}. \tag{31}$$

Figure 6 shows results for the case $\varepsilon_1 = \varepsilon_2 = 1$, $\varepsilon_3 = 80$, $R = R_1 = R_2$ with charges of the opposite ($q_1 = -q_2 = e$, Fig. 6a) and the same ($q_1 = q_2 = e$, Fig. 6b) sign. This corresponds to two ions solvated in water, where the ions are modelled as vacuum spheres with point charges in the center. When the distance of the spheres is large, the solution of the problem converges to the case of point charges with the polarization charges localized on them (discussed in Sec. 2.2). In this limit, $\varepsilon_{\text{eff}}(r) \rightarrow \varepsilon_3$ for $r \rightarrow \infty$. We have calculated the energy of the two sphere systems for $r/R = 2.25$, 2.5, 2.75, and 3 using various numbers of surface elements ($N = 256$, 484, 1024, and 1600). The effective dielectric coefficient is plotted as a function of $1/N$ (open circles). In the limit of "infinitely fine" grid ($1/N \rightarrow 0$), the analytical results obtained from Figs. 5b and 5d of the paper of Allen and Hansen [70] are also shown (filled circles). Increasing the number of tiles, our results converge to the analytical data.
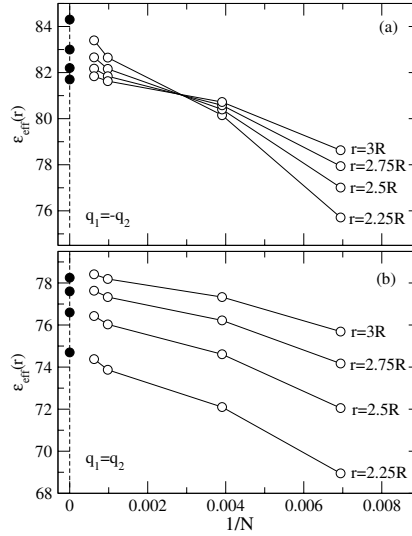

Figure 6. The effective dielectric coefficient as a function of $1/N$, where N is the number of tiles. Results are shown for charges of opposite (a) and equal (b) sign for different distances of the spheres. The filled circles are analytical results [70].

The convergence is quite slow, however. To explain this, the energies obtained for two specific cases with different fineness of grid are tabulated in Tab. 1. The small value of V_{int} is obtained from the sum of three large quantities: $V_{\text{int}} = W_e + W_i - W(\infty)$. For this reason, a small error in W_i or $W(\infty)$ causes a large error in V_{int}, and consequently, in ε_{eff}. The phenomenon of dielectric screening is well illustrated by these values. The large direct in-

Table 1. The various energies calculated for distance $r/R = 2.25$ for equal and opposite charges. The direct interaction between the charges is $W_e/kT = \pm 49.5140$. The analytical value for the energy of separated spheres is $W(\infty)/kT = -110.0139$ calculated from Eq. (31). The literature data for the effective dielectric coefficient is $\varepsilon_{eff} \sim 74.7$ and 84.3 for equal and opposite charges, respectively.

N	W_i/kT	$W(\infty)/kT$	V_{int}/kT	ε_{eff}
		$q_1 = q_2 = e$		
256	–158.8532	–110.0572	0.7181	68.95
484	–158.8739	–110.0466	0.6868	72.10
1024	–158.8799	–110.0362	0.6703	73.87
1600	–158.8801	–110.0318	0.6657	74.38
		$q_1 = -q_2 = e$		
256	–61.1972	–110.0572	–0.6540	75.71
484	–61.1504	–110.0466	–0.6176	80.15
1024	–61.1213	–110.0362	–0.5991	82.65
1600	–61.1114	–110.0318	–0.5937	83.4

teraction between the charges (W_e) is screened by a corresponding term raised by the polarization charges ($W_i - W(\infty)$). Note that for $W(\infty)$ the value obtained from our numerical method was used instead of the analytical value because the same numerical errors appear in both W_e and $W(\infty)$ which cancel each other. Using the analytical value for $W(\infty)$ results in a considerable overestimation of ε_{eff}.

In these two subsections, simple calculations for systems containing dielectric sphere(s) have been presented. Simulations for the distribution of ions around and within dielectric sphere(s) are under way.

3.4   *Ion channel geometry*

Ion channels are proteins with a narrow, highly selective pore in their center penetrating the cell membrane. They provide an effective and physiologically very important mechanism to control the pass of selected ions through the membrane. Calcium and sodium channels have crucial role in the function of nerve system, muscle contraction, and cell communication. The accurate 3D structure of these channels is unknown. However, the amino acid side chains that line the selectivity filter, which is a small and crowded region in the pore, are known. The selectivity of the channels is determined by these side chains which are 4 glutamate groups (EEEE locus) in the case of the calcium channel. Based on this minimal information a simple model for the calcium channel has been developed [37–43]. A small cylinder representing the filter is connected to baths that large enough for a bulk system to form in their middle. In this

study, the filter is embedded in a membrane (Fig. 7a). The two baths are connected to the filter through two cone shaped vestibules at the entries of the filter (these vestibules were absent in our earlier studies). The system has a rotational symmetry: the surfaces in the simulation cell form a surface of revolution around the centerline of the pore.
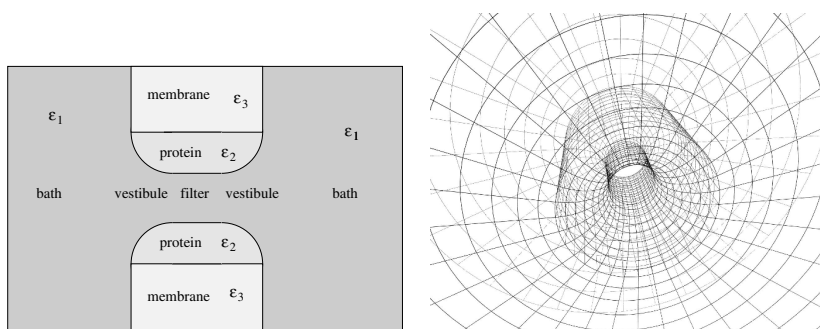

Figure 7. (a) The simulation cell for the ion channel geometry. (b) Illustration of the method to construct the grid on the dielectric boundary surfaces.

The dielectric coefficient was uniform ($\varepsilon = 80$) in our previous studies [39–42]. In this work, we present some MC results for the case where we allow various regions in the system to have different dielectric coefficient. Specifically, the membrane, the protein, and the electrolyte solution in which the ions move have dielectric coefficients $\varepsilon_3 = 2$, $\varepsilon_2 = 20$, and $\varepsilon_1 = 80$, respectively. The dielectric boundary surfaces that appear in the simulation cell have different geometries. Consequently, different u, v parameters are used for these surfaces. Due to the rotational symmetry, the variable ϕ is one of the parameters in all cases. The other parameter depends on the geometry of the various regions which are: (1) filter/protein and (2) protein/membrane boundaries – cylinders with z the second parameter, (3) vestibule/protein boundary – a cone shaped surface with a spherical curvature (an appropriate θ angle parametrize the curvature), and (4) bath/membrane boundary – planes perpendicular to the z-axis, the other parameter is r which is the distance from the rotational axis. The grid we constructed is illustrated in Fig. 7b; the grid is finest inside the filter (where important things happen) and it becomes coarser farther from the filter.

The whole simulation cell is confined by a large cylinder. The cell is finite, no periodic boundary conditions are applied. The radius of the cell is 60 Å, its length is 178.72 Å. These values are large enough so that the potential at the outer walls can be regarded as zero in average. The radius and length of the filter are 5 and 10 Å, respectively. The outer radius of the protein is 15 Å, its

length (that equals the width of the membrane) is 30 Å. This means that the curvature radius of the vestibules is 10 Å.

There are 8 half charged oxygen ions (with diameters 2.8 Å) in the filter representing the 4 unprotonated structural groups of the EEEE locus of the calcium channel. These ions are assumed to be mobile inside the filter but they are restricted to the filter. There are 100 sodium and 100 chloride ions (diameters 1.9 and 3.62 Å) in the system in appropriate numbers to obtain a 0.1 M NaCl solution in the bath. There are also 2 calcium ions (diameter 1.98 Å). Thus, the whole simulation cell is electroneutral.
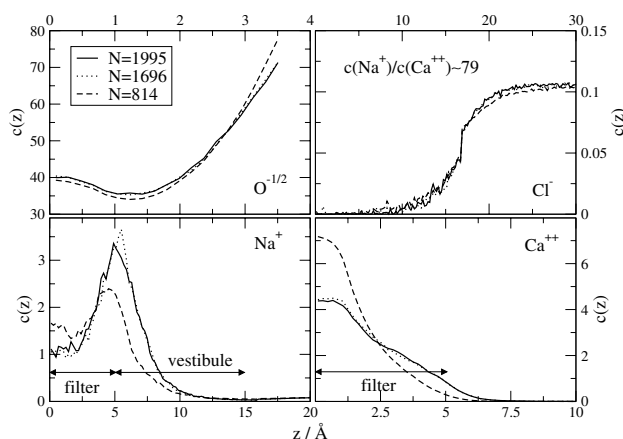

Figure 8. The concentration profiles for the various ionic species as obtained from MC simulations applying grids of different resolutions. The system is symmetric for the center plane of the membrane, so the results obtained for the left and right sides are averaged.

We present results of 3 simulations which differ from each other only in the resolution of the grid. The widths of the surface elements in the filter are 1.43, 1, and 0.91 Å, which correspond to total number of tiles $N = 814$, 1760, and 1995, respectively. The lengths of the simulations are 886 000, 339 000, and 308 000 MC cycles, respectively. Besides the usual particle displacements, biased particle exchanges between the channel and the baths were applied (for details, see [41, 42]).

The results for the density profiles (in mole/dm^3 unit) are shown in Fig. 8. Comparing the results to Fig. 7 of [41] (where a similar geometry was used but without dielectric boundaries), it can be seen that the presence of dielectric inhomogeneity has a large effect on the charge distribution in the channel. In our earlier study [41] both the Ca^{++} and Na$^+$ ions were concentrated in the center of the filter. On the contrary, our present results indicate that the Ca^{++}

ions tend to accumulate in the center of the filter, while the Na^+ ions are rather positioned at the entries of the filter and in the vestibules. This result clearly shows the importance of dielectric boundaries.

For this work, the important aspect of our simulation is the dependence of the results on the resolution of the grid. It is seen that our results converge as the number of surface elements is increased. For $N = 814$ the curves are quite different from those obtained for $N = 1696$ and 1995 although the qualitative behavior is the same. The curves obtained for the two better resolutions differ from each other only in minor details. This is in accordance with our earlier findings which showed that we can obtain accurate results from simulations if the dimensions of the surface elements are smaller than the closest approach of the ions to the surfaces. The SC/PC approximation was used in our simulations.

4. Summary

We have presented the ICC method with developments in which the polarization charges are treated as surface charges with a constant value inside a boundary element (SC approximation). We have discussed the effect of using the SC approximation to calculate the matrix elements and polarization energy for various geometries. It was shown that this approach is important not only for curved dielectric boundaries but also for flat boundaries if the are close to each other. On the examples of dielectric spheres, it was shown that using the SC approximation (or "curvature corrections") is especially important for curved surfaces. If the geometry of dielectric interfaces does not change during a simulation, the method can efficiently been used in computer simulations, as our results for an ion channel geometry do show.

References

[1] Miertus, S., Scrocco, E., and Tomasi, J. *Chem. Phys.*, 1981, **55**, p. 117.

[2] Tomasi, J., and Persico, M. *Chem. Rev.*, 1994, **94**, p. 2027.

[3] Klamt, A., and Schüürmann, G. *J. Chem. Soc. Perkin. Trans.*, 1993, **2**, p. 799.

[4] Mennucci, B., Cancès, E., and Tomasi, J. *J. Phys. Chem. B*, 1997, **101**, p. 10506.

[5] Mennucci, B., and Cancès, E. *J. Math. Chem.*, 1998, **23**, p. 309.

[6] Mennucci, B., Cammi, R., and Tomasi, J. *J. Chem. Phys.*, 1998, **109**, p. 2798.

[7] Hoshi, H., Sakurai, M., Inoue, Y., and Chûjô, R. *J. Chem. Phys.*, 1987, **87**, p. 1107.

[8] Cammi, R., and Tomasi, J. *J. Chem. Phys.*, 1994, **100**, p. 7495.

[9] Cammi, R., and Tomasi, J. *J. Chem. Phys.*, 1994, **101**, p. 3888.

[10] Pomelli, C.S., Tomasi, J., and Barone, V. *Theor. Chem. Acc.*, 2001, **105**, p. 446, (and references therein).

[11] Frediani, L., Cammi, R., Corni, S., and Tomasi, J. *J. Chem. Phys.*, 2004, **120**, p. 3893, (and references therein).

[12] Zauhar, R.J., and Morgan, R.S. *J. Comput. Chem.*, 1988, **9**, p. 171.

[13] Yoon, B.J., and Lenhoff, A.M. *J. Comput. Chem.*, 1990, **11**, p. 1080.

[14] Juffer, A.H., Botta, E.F.F., van Keulen, B.A.M., van der Ploeg, A., and Berendsen, H.J.C. *J. Comp. Phys.*, 1991, **97**, p. 144.

[15] Fox, T., Rösch, N., and Zauhar, R.J. *J. Comput. Chem.*, 1993, **14**, p. 253.

[16] Liang, J., and Subramaniam, S. *Biophys. J.*, 1997, **73**, p. 1830.

[17] Bordner, A.J., and Huber, G.A. *J. Comput. Chem.* **24**, 353 (2003).

[18] Chen, F., and Chipman, D.M. *J. Chem. Phys.*, 2003, **119**, p. 10289.

[19] Torrie, G.M., Valleau, J.P., and Patey, G.N. *J. Chem. Phys.*, 1982, **76**, p. 4615.

[20] Jacoboni, C., and Luigi, P. (1989). *The Monte Carlo Method for Semiconductor Device Simulation*. New York: Springer Verlag.

[21] Parsegian, V.A. *Nature (Lond.)*, 1969, **221**, p. 844.

[22] Neumcke, B., and Läuger, P. *Biophys. J.*, 1969, **9**, p. 1160.

[23] Hoyles, M., Kuyucak, S., and Chung, S.-H. *Phys. Rev. E*, 1998, **58**, p. 3654.

[24] Hoyles, M., Kuyucak, S., and Chung, S.-H. *Comput. Phys. Commun.*, 1998, **115**, p. 45.

[25] Chung, S.-H., Hoyles, M., Allen, T., and Kuyucak, S. *Biophys. J.*, 1998, **75**, p. 793.

[26] Chung, S.-H., Allen, T., Hoyles, M., and Kuyucak, S. *Biophys. J.*, 1999, **77**, p. 2517.

[27] Graf, P., Nitzan, A., Kurnikova, M., and Coalson, R. *J. Phys. Chem. B*, 1997, **101**, p. 5239.

[28] Levitt, D.G. *Biophys. J.*, 1978, **22**, p. 209; *ibid*, 1978, **22**, p. 221.

[29] Corry, B., Allen, T., Kuyucak, S., and Chung, S.-H. *Biophys. J.*, 2001, **80**, p. 195.

[30] Baştuĝ, T., and Kuyucak, S. *Biophys. J.*, 2003, **84**, p. 2871.

[31] Im, W., and Roux, B. *J. Chem. Phys.*, 2001, **115**, p. 4850.

[32] Schuss, Z., Nadler, B., and Eisenberg, R.S. *Phys. Rev. E*, 2001, **64**, p. 036116.

[33] Nadler, B., Hollerbach, U., and Eisenberg, R.S. *Phys. Rev. E*, 2003, **68**, p. 021905.

[34] Boda, D., Varga, T., Henderson, D., Busath, D.D., Nonner, W., Gillespie, D., and Eisenberg, B. *Mol. Sim.*, 2004, **30**, p. 89.

[35] Moy, G., Corry, B., Kuyucak, S., and Chung, S.-H. *Biophys. J.*, 2000, **78**, p. 2349.

[36] Corry, B., Kuyucak, S., and Chung, S.-H. *Biophys. J.*, 2000, **78**, p. 2364.

[37] Nonner, W., Catacuzzeno, L., and Eisenberg, B. *Biophys. J.*, 2000, **79**, p. 1976.

[38] Nonner, W., Gillespie, D., Henderson, D., and Eisenberg, B. *J. Phys. Chem. B*, 2001, **105**, p. 6427.

[39] Boda, D., Busath, D.D., Henderson, D., and Sokołowski, S. *J. Phys. Chem. B*, 2000, **104**, p. 8903.

[40] Boda, D., Henderson, D., and Busath, D.D. *J. Phys. Chem. B*, 2001, **105**, p. 11574.

[41] Boda, D., Henderson, D., and Busath, D.D. *Mol. Phys.*, 2002, **100**, p. 2361.

[42] Boda, D., Busath, D.D., Eisenberg, B., Henderson, D., and Nonner, W. *Phys. Chem. Chem. Phys.*, 2002, **4**, p. 5154.

[43] Gillespie, D., Nonner, W., and Eisenberg, R.S. *J. Phys.: Condens. Matt.*, 2002, **14**, p. 12129.

[44] Lu, J., and Green, M.E. *Progr. Colloid Polim. Sci.*, 1997, **103**, p. 121.

[45] Green, M.E., and Lu, J. *J. Phys. Chem. B*, 1997, **101**, p. 6512.

[46] Lu, J., and Green, M.E. *J. Phys. Chem. B*, 1999, **103**, p. 2776.

[47] Allen, R., Hansen, J.-P., and Melchionna, S. *Phys. Chem. Chem. Phys.*, 2001, **3**, p. 4177.

[48] Allen, R., Melchionna, S., and Hansen, J.-P. *Phys. Rev. Letters*, 2002, **89**, p. 175502.

[49] Allen, R., Melchionna, S., and Hansen, J.-P. *J. Phys.: Condens. Matter*, 2003, **15**, p. S297.

[50] Allen, R., Hansen, J.-P., and Melchionna, S. *J. Chem. Phys.*, 2003, **119**, p. 3905.

[51] Marcus, R.A. *J. Chem. Phys.*, 2956, **24**, p. 966; *ibid*, 1956, **24**, p. 979.

[52] Felderhof, B.U. *J. Chem. Phys.*, 1977, **67**, p. 493.

[53] Attard, P. *J. Chem. Phys.*, 2003, **119**, p. 1365.

[54] Löwen, H., Hansen, J.-P., and Madden, P.A. *J. Chem. Phys.*, 1993, **98**, p. 3275.

[55] York, D.M., and Karplus, M. *J. Phys. Chem. A*, 1999, **103**, p. 11060.

[56] Marchi, M., Borgis, D., Levy, N., and Ballone, P. *J. Chem. Phys.*, 2001, **114**, p. 437.

[57] HaDuong, T., Phan, S., Marchi, M., and Borgis, D. *J. Chem. Phys.*, 2002, **117**, p. 541.

[58] Boda, D., Gillespie, D., Nonner, W., Henderson, D., and Eisenberg, B. *Phys. Rev. E*, 2004, **69**, p. 046702.

[59] Nonner, W., and Gillespie, D. *Biophys. J.*, 2004, (in preparation).

[60] Jackson, J.D. (1999). *Classical Electrodynamics*, 3rd ed. New York: Wiley.

[61] Chipman, D.M., and Dupuis, M. *Theor. Chem. Acc.*, 2002, **107**, p. 90.

[62] Allen, M.P., and Tildesley, D.J. (1987). *Computer Simulation of Liquids*. New York: Oxford.

[63] Frenkel, D., and Smit, B. (1996). *Understanding Molecular Simulations*. San Diego: Academic Press.

[64] Sadus, R.J. (1999). *Molecular Simulation of Fluids; Theory, Algorithms, and Object-Orientation*. Amsterdam: Elsevier.

[65] Schlick, T. (2002). *Molecular Modeling and Simulation*. New York: Springer Verlag.

[66] Allen, R., and Hansen, J.-P. *Mol. Phys.*, 2003, **101**, p. 1575.

[67] Born, M. *Z. Phys.*, 1920, **1**, p. 45.

[68] Kirkwood, J.G. *J. Chem. Phys.*, 1934, **2**, p. 351.

[69] Onsager, L. *J. Am. Chem. Soc.*, 1936, **58**, p. 1586.

[70] Allen, R., and Hansen, J.-P. *J. Phys.: Condens. Matter*, 2002, **14**, p. 11981.